MOSSET, A., BONNET, J.-J. & GALY, J. (1978). *Z. Kristallogr.* **148**, 165–177.
NAKAI, I. (1986). *Am. Mineral.* **71**, 1236–1239.
NICHOLS, M. C. (1966). *Am. Mineral.* **51**, 267.
PABST, A. (1959). *Acta Cryst.* **12**, 733–739.
PARISE, J. B. & HYDE, B. G. (1986). *Acta Cryst.* C**42**, 1277–1280.
PERTLIK, F. (1975). *Tschermaks Mineral. Petrogr. Mitt.* **22**, 211–217.
PIRET, P., DECLERCQ, J.-P. & WAUTER-STOOP, D. (1980). *Bull. Minéral.* **103**, 176–178.
PIRET, P. & DELIENS, M. (1988). *Bull. Minéral.* **111**, 167–171.
PIRET, P., DELIENS, M. & PIRET-MEUNIER, J. (1985). *Can. Mineral.* **23**, 35–42.
QURASHI, M. M. & BARNES, W. H. (1963). *Can. Mineral.* **7**, 561–577.
RIBBE, P. H., GIBBS, G. V. & HAMIL, M. M. (1977). *Am. Mineral.* **62**, 807–811.
ROBERTSON, B. E. & CALVO, C. (1968). *Can. J. Chem.* **46**, 605–611.
ROSENZWEIG, A. & RYAN, R. R. (1975). *Am. Mineral.* **60**, 448–453.
ROSS, M., EVANS, H. T. JR & APPLEMAN, D. E. (1964). *Am. Mineral.* **49**, 1603–1621.
SABELLI, C. (1980). *Z. Kristallogr.* **151**, 129–140.
SABELLI, C. (1982). *Am. Mineral.* **67**, 388–393.
SABELLI, C. & ZANAZZI, P. F. (1968). *Acta Cryst.* B**24**, 1214–1221.
SABELLI, C. & ZANAZZI, P. F. (1972). *Acta Cryst.* B**28**, 1182–1189.
SHANNON, R. D. (1976). *Acta Cryst.* A**23**, 751–767.
SHANNON, R. D. & CALVO, C. (1972). *Can. J. Chem.* **50**, 3944–3949.
SHANNON, R. D. & CALVO, C. (1973). *Acta Cryst.* B**29**, 1338–1345.
SHOEMAKER, G. L., ANDERSON, J. B. & KOSTINER, E. (1977). *Am. Mineral.* **62**, 1042–1048.
SHOEMAKER, G. L., ANDERSON, J. B. & KOSTINER, E. (1981). *Am. Mineral.* **66**, 169–175.
SHOEMAKER, G. L. & KOSTINER, E. (1981). *Am. Mineral.* **66**, 176–181.
SIEBER, N. H., HOFMEISTER, W., TILLMANS, E. & ABRAHAM, K. (1984). *Fortschr. Mineral.* **62**, 231–233.
SÜSSE, P. (1972). *Z. Kristallogr.* **135**, 34–55.
SUTOR, D. J. (1967). *Acta Cryst.* **23**, 418–422.
TILLMANNS, E., HOFMEISTER, W. & PETITJEAN, K. (1985). *Bull. Geol. Soc. Finl.* **57**, 119–127.
TOMAN, K. (1977). *Acta Cryst.* B**33**, 2628–2631.
WILDNER, M. & GIESTER, G. (1988). *Mineral. Petrol.* **39**, 201–209.
WINTER, J. K. & GHOSE, S. (1979). *Am. Mineral.* **64**, 573–586.
ZAHROBSKY, R. F. & BAUR, W. H. (1968). *Acta Cryst.* B**24**, 508–513.
ZIGAN, F., JOSWIG, W. & SCHUSTER, H. D. (1977). *Z. Kristallogr.* **145**, 412–426.
ZIGAN, F. & SCHUSTER, H. D. (1972). *Z. Kristallogr.* **135**, 416–436.

Acta Cryst. (1993). B**49**, 56–62

Space-Group Determination of Human Tooth-Enamel Crystals

BY E. F. BRÈS*

Max-Planck-Institut für Metallforschung, Institut für Werkstoffwissenschaft, Seestrasse 92, *D* 7000 *Stuttgart* 1, *Germany*

D. CHERNS AND R. VINCENT

*H. H. Wills Physical Laboratory, University of Bristol, Bristol BS*8 1*TL, England*

AND J.-P. MORNIROLI

Laboratoire de Métallurgie Physique, Université de Lille 1, *Bâtiment C*6, 59 655 *Villeneuve d'Asc CEDEX, France*

(*Received* 9 *February* 1992; *accepted* 19 *June* 1992)

Abstract

In the present work, we have determined the space group of human tooth-enamel crystals using – for the first time for a biological crystal – convergent beam electron diffraction (CBED). The symmetries observed in the different patterns we have obtained lead us to the $P6_3/m$ hydroxyapatite space group. Disorder, most likely situated in the columns formed by the hydroxyl ions of the crystals, is suggested as a cause of weak intensity in the otherwise forbidden $000l$ (l odd) reflections and low visibility of first-order Laue zone (FOLZ) reflections in the CBED pattern from crystals oriented along the [0001] zone axis. A monoclinic phase was not observed.

Introduction

Human enamel is 96% by weight composed of an inorganic phase (Sicher, 1962), which consists of poorly crystalline carbonated hydroxyapatite crystals with an elongated prismatic shape (Voegel, 1978).

Hydroxyapatite (OHAP) is a mineral of chemical composition $Ca_4(1)Ca_6(2)(PO_4)_6(OH)_2$, whose Ca atoms occupy two series of nonequivalent sites; the

* On leave from INSERM U157, Faculté de Chirurgie Dentaire, Université Louis Pasteur, 1 place de l'Hôpital, 67000 Strasbourg, France.

0108-7681/93/010056-07$06.00

Ca(1) in the fourfold symmetry 4(*f*) position and the Ca(2) in the sixfold symmetry 6(*h*) position. The OH groups occupy disordered positions above or below the triangles formed by the Ca(2) atoms (Kay, Young & Posner, 1964). The disorder of the OH groups gives rise to a 'macroscopic' space group $P6_3/m$ (as determined by X-ray diffractometry), which is lost at the level of the individual columns. OHAP has a dipyramidal hexagonal prismatic morphology, while tooth-enamel crystals have an elongated hexagonal prismatic shape. The average dimensions of the section parallel to the enamel crystal basal plane are 90 × 50 nm (Voegel, 1978). The structure of OHAP as determined by X-ray diffractometry is given in Fig. 1 and Table 1.

Numerous studies of OHAP and tooth-enamel crystals using high-resolution electron microscopy (HREM) at a Scherzer resolution of 0.25 nm (Brès, Barry & Hutchison, 1985; McLean & Nelson, 1982; Nelson, McLean & Sanders, 1983; Ichijo, Yamashita & Akahori, 1984; Ichijo & Yamashita, 1983; Ichijo, 1983; Kanaya, Baba, Shinohara & Ichijo, 1984), at a Scherzer resolution of 0.20 nm (Brès, Voegel & Frank, 1990) and at a Scherzer resolution of 0.17 nm (Barry & Brès, 1987) have shown a good structure correspondence between the structures of OHAP and enamel crystals. However, a difference between calculated and experimental image details has been observed in the *c* direction of the $[\bar{1}2\bar{1}0]$ and $[1\bar{1}00]$ images (Brès *et al.*, 1985). Recently, the loss of the sixfold hexagonal symmetry was observed in enamel apatite crystals aligned along the [0001] zone axis (Brès *et al.*, 1990; Brès, Steuer, Voegel, Frank & Cuisinier, 1992). All these deviations from the hydroxyapatite hexagonal structure are difficult to interpret by HREM, as this method gives limited symmetry information. In the present study, we determine the space group of human tooth-enamel crystals by electron diffraction. This represents the first CBED study of biological crystals.

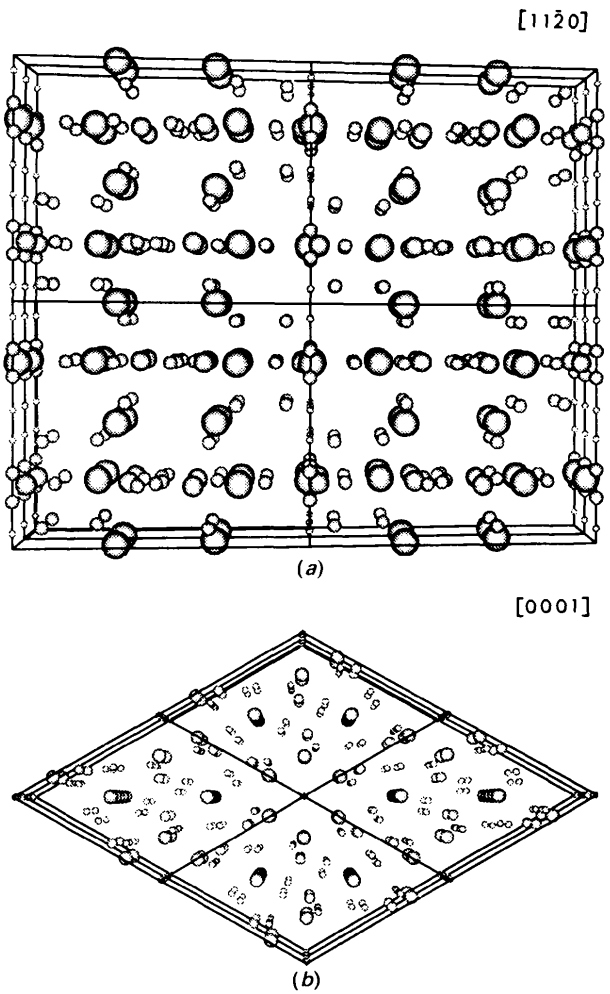

Fig. 1. Structure of OHAP viewed along (*a*) the [11$\bar{2}$0] direction and (*b*) along the [0001] direction. In both cases, two by two unit cells are shown. Ca, P, O and H atoms are shown as spheres of decreasing size.

Table 1. *Crystallographic parameters of hydroxyapatite (Kay, Young & Posner, 1964)*

'occ' means occupancy.

Lattice	Hexagonal, with lattice parameters: $a_1 = a_2 = a_3 = 0.9432$ nm, $c = 0.6881$ nm and two formula units per cell.
Space group	$P6_3/m$ (No. 176).
Atomic coordinates	O(1) in 6(*h*): 0.3272, 0.4837, $\frac{1}{4}$, occ = 1
	O(2) in 6(*h*): 0.5899, 0.4666, $\frac{1}{4}$, occ = 1
	O(3) in 12(*i*): 0.3457, 0.2595, 0.0736, occ = 1
	P in 6(*h*): 0.3999, 0.3698, $\frac{1}{4}$, occ = 1
	Ca(1) in 4(*f*): $\frac{1}{3}$, $\frac{2}{3}$, 0.0010, occ = 1
	Ca(2) in 6(*h*): 0.2464, 0.9938, $\frac{1}{4}$, occ = 1
	O_H in 4(*e*): 0.0, 0.0, 0.1930, occ = $\frac{1}{2}$
	H in 4(*e*): 0.0, 0.0, 0.0617, occ = $\frac{1}{2}$

Experimental

Human enamel was obtained from several non-carious human teeth of 20–50 year old patients, dissected into small 1–2 mm blocks and fixed for 3 h in a 2% glutaraldehyde–paraformaldehyde solution in a 0.1 *M* cacodylate buffer at pH 7.4. After 1 h postfixation in a 2% osmic acid solution in the same buffer, the fragments were embedded in Epon 812. Nondecalcified sections were obtained with a Sorvall–Porter ultramicrotome equipped with a diamond knife. In order to reduce noise as well as chemical reactions with the supporting film, the sections were deposited onto holey carbon films and the crystals selected for the observation were those lying above holes.

The specimens were examined at accelerating voltages ranging from 100 to 250 kV with Philips EM430

ST (Strasbourg) and EM430 T (Bristol) microscopes equipped with either Gatan double-tilt liquid-nitrogen cooling holders or Philips standard-tilt/rotation holders.

The simulation of the diffraction patterns was performed with the *EMS* suite of computer programs (Stadelmann, 1987) as well as the program developed by Morniroli (1989).

Results

Consider first the geometry of the Bravais lattice. Reflections in the zero layer of [0001] CBED patterns are arranged in a triangular net (Fig. 2). Although the first-order Laue zone (FOLZ) reflections are not visible in zone-axis patterns, experiments where the crystals are tilted off the c axis excite idential triangular nets of reflections in adjacent layers of the reciprocal lattice (Fig. 3). These nets are stacked directly above each other, consistent with a P-type hexagonal or trigonal lattice, and not in the $ABC...$ sequence expected for a cubic or rhombohedral lattice aligned along $\langle 111 \rangle$. This identification of a P lattice is confirmed by the relative displacement of $1/2a^*$ observed between zero-order and first-order nets of reflections in $\langle 11\bar{2}0 \rangle$ patterns (Fig. 4).

The projection symmetry of the zero-layer reflections in [0001] CBED patterns shows a sixfold rotation, with a clear absence of mirror planes parallel to the c axis. No reflections are visible in the FOLZ, even when the specimen is cooled with liquid nitrogen, nor is any corresponding detail visible within the zero-layer discs.

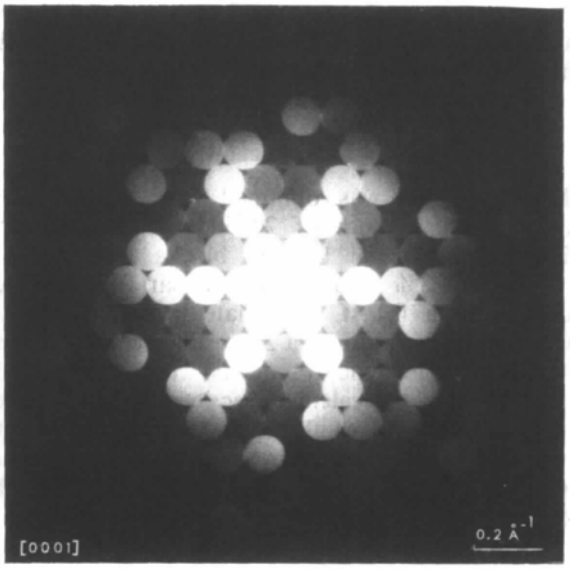

Fig. 2. CBED ZOLZ pattern of a human tooth-enamel crystal oriented along the [0001] zone axis; sixfold symmetry with no mirror is observed.

CBED aligned on a $\langle 11\bar{2}0 \rangle$ axis shows $2mm$ projection symmetry, where only weak intensity is visible within the $000l$ (l odd) reflections (Fig. 5). However, examination of the FOLZ reflections around the $\langle 11\bar{2}0 \rangle$ axis showed that the whole pattern symmetry is reduced to a single mirror parallel to the (0001) basal plane (Fig. 4).

Determination of the space group

The hexagonal and trigonal crystal classes include only three point groups which show sixfold projec-

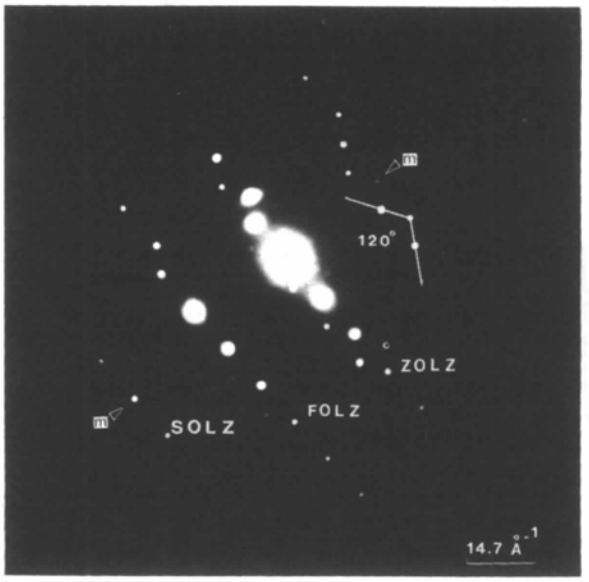

Fig. 3. CBED ZOLZ pattern of a human tooth-enamel crystal oriented along the [11$\bar{2}$0] zone axis; $2mm$ symmetry is observed.

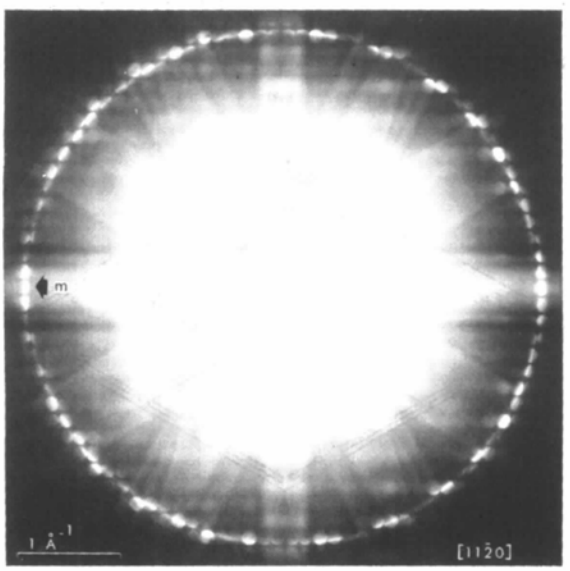

Fig. 4. CBED FOLZ pattern of a human tooth-enamel crystal viewed along the [11$\bar{2}$0] zone axis; m symmetry is observed.

tion symmetry with no mirror planes parallel to c; these are the 6, $6/m$ and 3 point groups. However, only the hexagonal point group, $6/m$, includes the basal plane mirror observed in FOLZ reflections around $\langle 11\bar{2}0 \rangle$.

There are only two possible space groups, $P6/m$ and $P6_3/m$, consistent with point group $6/m$. In principle, these two space groups are distinguished by the presence or absence of dark bars (Gjønnes–Moodie lines of absence; Gjønnes & Moodie, 1965) with reflections of the type $000l$ (l odd) that have no zero structure factor if a 6_3 screw axis is present. However, the contrast observed in these reflections (Fig. 5) is rather ambiguous, with no clear evidence that the intensity drops to zero along the line parallel to g through the centre of the discs. In these circumstances, we can only infer that the ideal space group may be $P6_3/m$, but there exists some disorder on an atomic scale that reduces the symmetry imposed by the translation element in the 6_3 screw axis.

Discussion

Are human tooth-enamel crystals monoclinic or hexagonal?

A structural phenomenon specific to hydroxyapatite has been reported by Elliot, Mackie & Young (1973). These authors have shown that the X-ray diffraction patterns of hydroxyapatite crystals prepared from essentially stoichiometric chlorapatite single crystals heated in steam for two weeks exhibit extra reflections explicable on the basis of the $P2_1/b$ space group for hydroxyapatite and by a series of twin-related 120° rotations about the c axis. The specimen examined by these authors was approximately 63% hexagonal and 37% monoclinic, with an even distribution in the monoclinic phase of all twin elements. The monoclinic cell with the $P2_1/b$ space group is related to the usual one for hydroxyapatite by a translation of b(hex)/2 as well as by doubling one of the hexagonal axes (b).

A particular point of interest about a monoclinic form of hydroxyapatite arises from the reported bioelectric effect whereby crystal growth is influenced by an electric current or field (Basset, Pawluk & Becker, 1964), which is of course not possible in centrosymmetric hexagonal crystals. However, due to experimental difficulties three-dimensional structure studies of crystals in calcified tissues have not yet been carried out. One problem encountered is the necessity of using probes smaller than a single monoclinic domain, the other lies in the need for three-dimensional information. Because of the b/a ratio of the lattice parameters and the absence of reflections forbidden by the glide plane, $P2_1/b$ monoclinic apatite crystals oriented along the [001] zone axis give zero-order Laue zone (ZOLZ) patterns with apparent sixfold symmetry, not differentiable from ZOLZ patterns for [0001] oriented $P6_3/m$ hexagonal

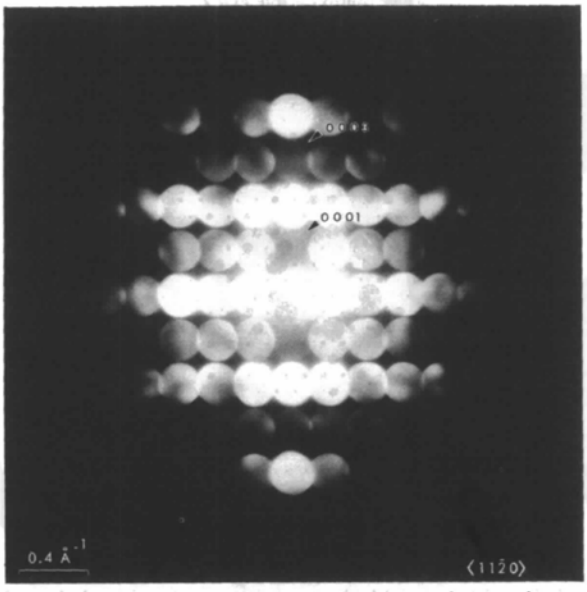

Fig. 5. Higher-order Laue zones of a human tooth-enamel crystal oriented close to the [0001] zone axis.

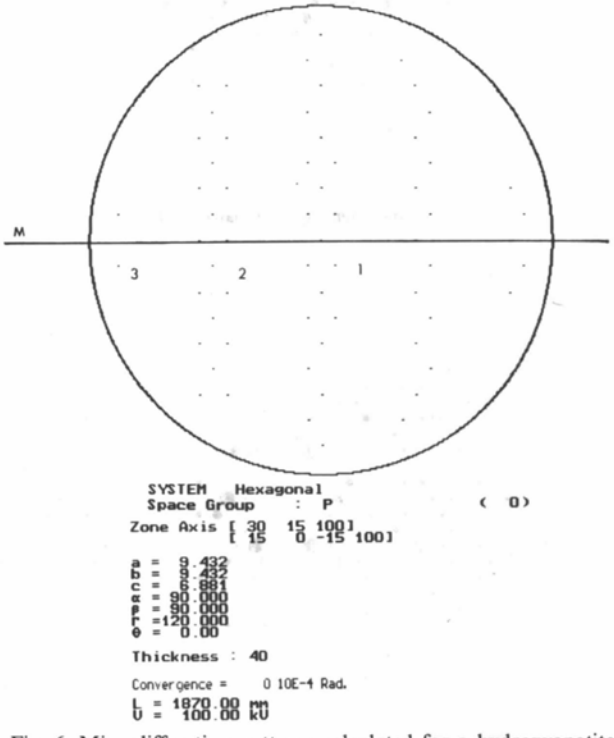

Fig. 6. Microdiffraction patterns calculated for a hydroxyapatite crystal tilted slightly away from the [0001] zone axis and along one of the mirrors. The numbers '1', '2' and '3' indicate, respectively, the ZOLZ, FOLZ and SOLZ (second-order Laue zone) patterns.

crystals in terms of geometry alone. The geometry of FOLZ reflections obtained from $P2_1/b$ monoclinic apatite crystals oriented along the [001] zone axis is reduced to twofold due to the presence of reflections absent in the zero layer, whereas the FOLZ symmetry round [0001] for $P6_3/m$ hydroxyapatite crystals remains sixfold (Fig. 6). However, when FOLZ patterns from all three twin elements described by Elliott *et al.* (1973) are sampled together, the combined pattern shows sixfold symmetry as observed for hexagonal hydroxyapatite crystals, but the scale is reduced by a factor of two due to the presence of extra reflections (Fig. 7).

The combination of a small probe size (down to 5 nm) with three-dimensional ZOLZ + FOLZ reflections implies that CBED is well suited for the detection of monoclinic crystals in human calcified-tissue crystals. In this study, the visibility of the FOLZ reflections around [0001] oriented crystals is very poor and the geometry of successive layers in the reciprocal lattice is obtained by tilting the crystals a few degrees off from the [0001] zone axis (Fig. 3). In these patterns, identical triangular nets of reflections are observed, consistent with the Bravais lattice of hexagonal hydroxyapatite and not the equivalent pattern of monoclinic hydroxyapatite shown in Fig. 7 or the hexagonal pattern produced by a 120° twinned crystal (Fig. 8).

This seems to indicate that the crystals observed are not monoclinic but hexagonal. However, as

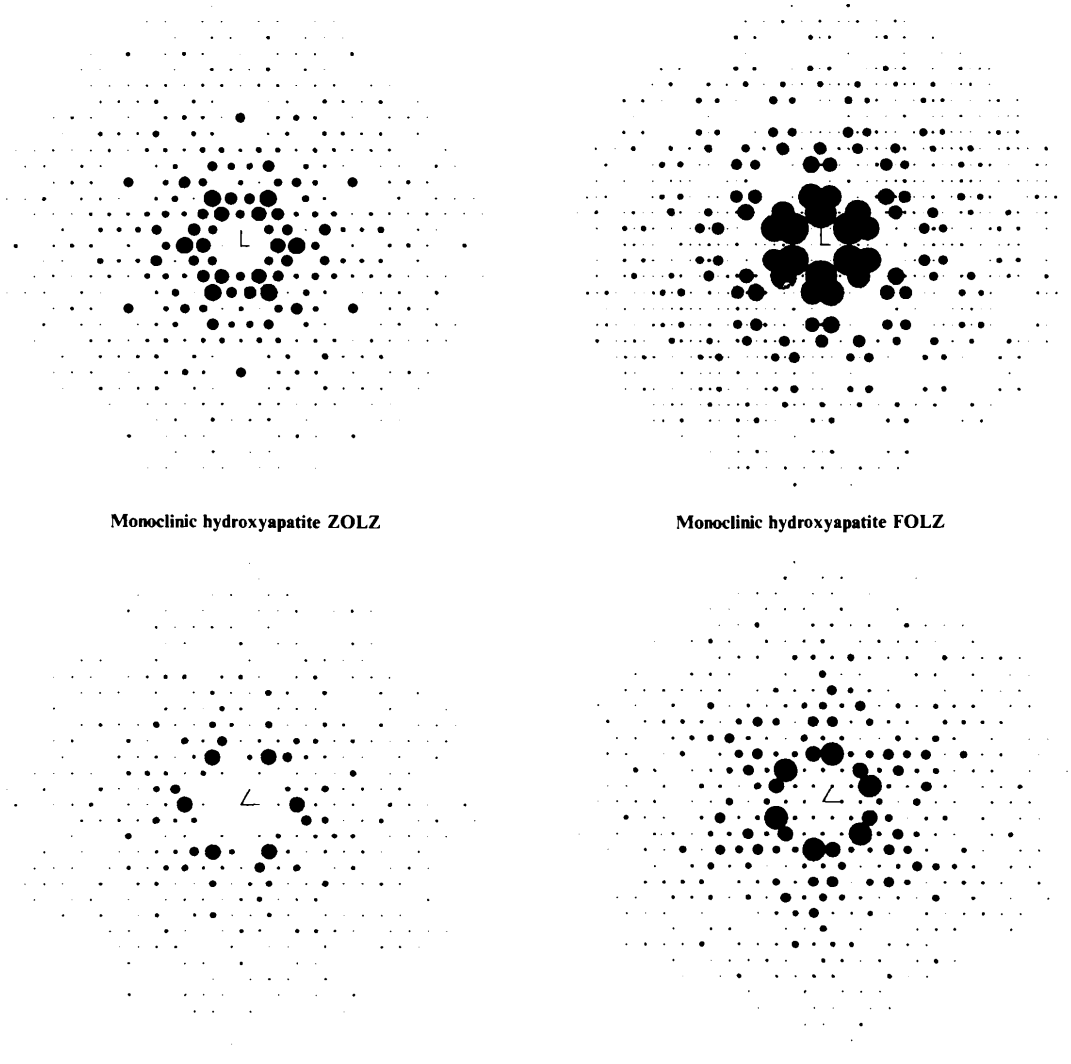

Fig. 7. ZOLZ and FOLZ microdiffraction patterns calculated for monoclinic and hexagonal hydroxyapatite crystals oriented along the [0001] zone axis.

stated by Elliott *et al.* (1973), only 37% of the crystals they observed were monoclinic, so more observations are still required before any possibility of a monoclinic structure in tooth-enamel crystals can be ruled out.

The presence of a weak intensity in the 000*l* (*l odd*) *reflections*

The weak intensity observed in the 000l (*l* odd) reflections could have several causes, most probably connected with disorder along the screw axis. The $P6_3/m$ hydroxyapatite space group is valid at the macroscopic level for description of the average structure because of the equal probability for positioning of the hydroxyl ions above or below the triangles formed by the Ca(2) atoms. This statistical averaging is most probably lost in the short range, as adjacent hydroxyl ions would then be too close to each other. The shifting of hydroxyl ions from one side to the other of the Ca(2) triangles is caused either by interstitial F^- ions, O^{2-} ions or H_2O molecules, or by the direct replacement of two hydroxyl ions by one CO_3^{2-} ion accompanied by a space-group transformation from $P6_3/m$ to *Pb* (Elliot, Bonel & Trombe, 1980).

The ion concentration necessary for this shifting varies from 15 to 16% in chlorapatite (Prener, 1967). Ionic vacancies along the (OH) column probably have a more important effect on the ionic disposition along this column, as a loss of 7% of the Cl^- ions from the chlorapatite structure accompanied by an equivalent loss of Ca^{2+} ions results in a transformation from a hexagonal to a monoclinic structure.

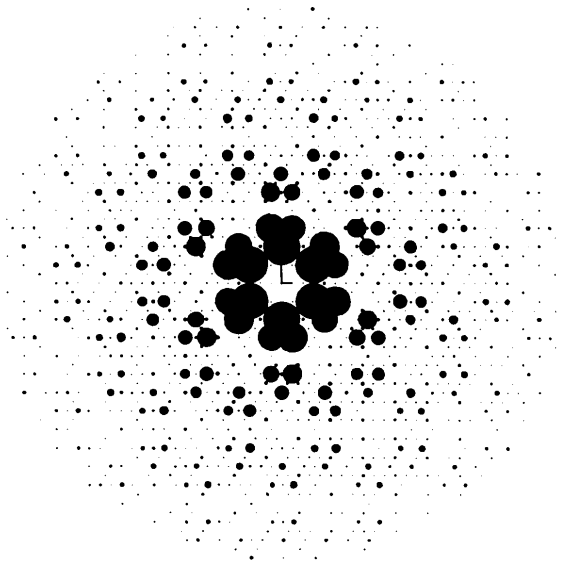

Fig. 8. FOLZ microdiffraction patterns calculated for a monoclinic hydroxyapatite crystal with 120° twins and oriented along the [0001] zone axis.

Given the probe size used (10–50 nm), it is unlikely that the variations in positioning of the hydroxyl ions would be observed or, more strictly speaking, that the proportion of hydroxyl ions above or below the Ca(2) triangle would differ, which would result in both a loss of the /*m* mirror plane and of the 6_3 screw axis.

Concluding remarks

In the present work, we have determined the space group of human tooth-enamel crystals, the first such determination for a biological crystal. The results obtained are consistent with the $P6_3/m$ space group for hydroxyapatite. Although a small probe (5 nm) was used to exite the FOLZ reflections, no evidence was found for the presence of a monoclinic phase as described by Elliott *et al.* (1973). Probable disorder in the columns formed by the hydroxyl ions of the crystals may account for weak intensities in the otherwise forbidden 000*l* (*l* odd) reflections and the poor visibility of FOLZ reflections in the CBED pattern of crystals oriented along the [0001] zone axis.

E. F. Brès would like to thank the Alexander von Humbolt Foundation for a Fellowship.

References

BARRY, J. C. & BRÈS, E. F. (1987). *Proc. Electron Microsc. Soc. Am. 43rd Ann. Meeting*, edited by G. W. BAILEY, pp. 170–171. San Francisco: San Francisco Press.

BASSETT, C. A., PAWLUK, R. J. & BECKER, R. O. (1964). *Nature (London)*, **204**, 652–654.

BRÈS, E. F., BARRY, J. C. & HUTCHISON, J. L. (1985). *J. Ultrastruct. Res.* **20**, 261–274.

BRÈS, E. F., STEUER, P., VOEGEL, J.-C., FRANK, R. M. & CUISINIER, F. (1992). *J. Microsc. (Oxford)*. Submitted.

BRÈS, E. F., VOEGEL, J.-C. & FRANK, R. M. (1990). *J. Microsc. (Oxford)*, **160**, 183–201.

ELLIOTT, J. C., BONEL, G. & TROMBE, J. C. (1980). *J. Appl. Cryst.* **13**, 618–621.

ELLIOTT, J. C., MACKIE, P. E. & YOUNG, R. A. (1973). *Science*, **180**, 1055–1057.

GJØNNES, J. & MOODIE, A. F. (1965). *Acta Cryst.* **19**, 65–67.

ICHIJO, T. (1983). *Jpn. J. Oral Biol.* **25**, 615–634.

ICHIJO, T. & YAMASHITA, Y. (1983). *Mechanisms of Tooth Enamel Formation*, edited by S. SUGA, pp. 205–218. Tokyo: Quintessence.

ICHIJO, T., YAMASHITA, Y. & AKAHORI, Y. (1984). *Tooth Enamel* IV, edited by R. W. FEARNHEAD & S. SUGA, pp. 68–72. Amsterdam: Elsevier.

KANAYA, K., BABA, N., SHINOHARA, C. & ICHIJO, T. (1984). *Micron Microsc. Acta*, **15**, 17–35.

KAY, M. I., YOUNG, R. A. & POSNER, A. S. (1964). *Nature (London)*, **204**, 1050–1052.

MCLEAN, J. D. & NELSON, D. G. A. (1982). *Micron*, **13**, 409–413.

MORNIROLI, J.-P. (1989). *EMAG-MICRO89*, *Inst. Phys. Conf. Ser.* No. 98, 87–89.

NELSON, D. G. A., MCLEAN, J. D. & SANDERS, J. V. (1983). *J. Ultrastruct. Res.* **84**, 1–15.

PRENER, J. S. (1967). *J. Electrochem. Soc.* **114**, 77–83.
SICHER, H. (1962). *Oral Histology and Embryology*. St Louis: Mosby.
STADELMANN, P. A. (1987). *Ultramicroscopy*, **21**, 131–146.
VOEGEL, J.-C. (1978). PhD thesis, Univ. Louis Pasteur, Strasbourg, France.

Acta Cryst. (1993). B**49**, 62–66

Structural Parameters and Electron Difference Density in Y_2BaCuO_5

BY R. H. BUTTNER AND E. N. MASLEN

Physics Department, University of Western Australia, Nedlands, WA 6009, *Australia*

(*Received* 5 *February* 1992; *accepted* 21 *July* 1992)

Abstract

Diyttrium barium copper(II) pentoxide, Y_2BaCuO_5, $M_r = 458.7$, orthorhombic, *Pnma*, $a = 12.188$ (2), $b = 5.662$ (2), $c = 7.132$ (2) Å, $V = 492.17$ (3) Å^3, $Z = 4$, $D_x = 6.19$ Mg m^{-3}, λ(Mo $K\alpha$) = 0.71069 Å, $\mu = 36.633$ mm^{-1}, $F(000) = 812$, $T = 298$ K, final $R = 0.059$, $wR = 0.028$ for 2758 unique reflections. The structural parameters for the nonsuperconducting 'green phase' Y_2BaCuO_5 were redetermined and the electron density compared with that for the high-T_c superconductor $YBa_2Cu_3O_{7-\delta}$. The $\Delta\rho$ topography near Cu in Y_2BaCuO_5 resembles that near Cu2 in $YBa_2Cu_3O_{7-\delta}$, which has similar coordination. It differs markedly from that near Cu1, which coordinates with disordered O atoms. The similarity of both coordination and electron density for the Cu atom in the green phase with those for Cu2 in the high-T_c compound is consistent with both atoms being in the +2 oxidation state.

Introduction

A nonsuperconducting green phase with the composition Y_2BaCuO_5 was first identified as a contaminant in the high-temperature superconductor $YBa_2Cu_3O_{7-\delta}$. A powder investigation by Michel & Raveau (1982) tentatively established the space group of Y_2BaCuO_5 to be *Pbnm*, which was confirmed in single-crystal studies by Watkins, Fronczek, Wheelock, Goodrich, Hamilton & Johnson (1988) and by Sato & Nakada (1989). The atomic positions for the two earlier studies were concordant, but the Y1 and Y2 vibration amplitudes from the first are markedly smaller than those from the second. Because Y_2BaCuO_5 is not affected by nonstoichiometry or disorder, its structural geometry and $\Delta\rho$ topography can be usefully compared with those of the Cu atoms in the high-T_c compound. A further objective for a more accurate study is to check the vibration amplitudes.

Table 1. *Experimental and refinement data for* Y_2BaCuO_5

Scan type	$\omega/2\theta$
Scan speed	6.51° min^{-1}
Peak scan width ($a + b\tan\theta$)	1.64; 0.71°
Maximum 2θ	100°
Maximum variation in intensity of standards $\pm 600 \pm 040 \pm 004$	1.3%
Number of reflections measured	22779
Transmission range in absorption corrections	0.23; 0.36
R_{int} (before and after absorption)	0.086; 0.071
Number of independent reflections $0 \le h \le 26$, $0 \le k \le 12$, $0 \le l \le 15$	2758
R	0.059
wR	0.028
S	1.66 (2)
Maximum height in final difference Fourier map	7.6 (9) e Å^{-3}
Minimum height in final difference Fourier map	−6.6 (9) e Å^{-3}
Minimum extinction y	0.67

With the assumption of the normal oxidation states of +2 for Ba, +3 for Y and −2 for O, charge balance requires that Cu for Y_2BaCuO_5 be in the +2 state. Nevertheless, its fivefold coordination closely resembles that of Cu2 in $YBa_2Cu_3O_{7-\delta}$, frequently cited as having an oxidation number that approaches +3 as δ decreases from 0.5. Some theoretical treatments relate the superconductivity of the high-T_c material to the Cu2-atom oxidation number. In that context the electron density near the Cu atom in the stoichiometric compound Y_2BaCuO_5 provides a reference standard.

Buttner & Maslen (1992) have recently shown that $\Delta\rho$ maps for the high-temperature superconductor $YBa_2Cu_3O_{7-\delta}$ are related to the structural geometry. The $\Delta\rho$ topography near the Cu1 atom adjacent to the O-atom defects is similar to that near atoms with elongated octahedral coordination in well defined +2 states such as Cu in $KCuF_3$ (Buttner, Maslen & Spadaccini, 1990). On the other hand, the electron density near Cu2, which has fivefold coordination and is not affected directly by oxygen disorder, has

0108-7681/93/010062-05$06.00